

# Impact of Multiple Radar reflectivity data assimilation on the numerical simulation of a Flash Flood Event during the HyMeX campaign

Ida Maiello<sup>1,2</sup>, Sabrina Gentile<sup>3,1</sup>, Rossella Ferretti<sup>2</sup>, Luca Baldini<sup>4</sup>, Nicoletta Roberto<sup>4</sup>, Errico Picciotti<sup>2,5</sup>, Pier Paolo Alberoni<sup>6</sup>, Frank Silvio Marzano<sup>1,2</sup>

<sup>1</sup>Department of Information Engineering, Electronics and Telecommunications - Sapienza University of Rome, Rome, Italy

<sup>2</sup>CETEMPS, Department of Physical and Chemical Sciences - University of L'Aquila, L'Aquila, Italy

<sup>3</sup>Institute of Methodologies for Environmental Analysis, CNR IMAA, Potenza, Italy

<sup>4</sup>Institute of Atmospheric Sciences and Climate, CNR ISAC, Roma, Italy

<sup>5</sup>Himet s.r.l, L'Aquila, Italy

<sup>6</sup>Arpa Emilia Romagna - Servizio Idro-Meteo-Clima, Bologna, Italy

*Correspondence to:* Ida Maiello (ida.maiello@aquila.infn.it)

**Abstract.** An analysis to evaluate the impact of multiple radar reflectivity data with a three dimensional variational (3D-Var) assimilation system on a heavy precipitation event is presented. The main goal is to build a regionally-tuned numerical prediction model and a decision-support system for environmental civil protection services and demonstrate it in the central Italian regions, distinguishing which type of observations, conventional and not (or a combination of them) is more effective in improving the accuracy of the forecasted rainfall. In that respect, during the first Special Observation Period (SOP1) of HyMeX (Hydrological cycle in the Mediterranean Experiment) campaign several Intensive Observing Periods (IOPs) were launched and nine of which occurred in Italy. Among them, IOP4 is chosen for this study because of its low predictability regarding the exact location and amount of precipitation. This event hit central Italy on 14 September 2012 producing heavy precipitation and causing several damages to buildings, infrastructures and roads. Reflectivity data taken from three C-band Doppler radars running operationally during the event are assimilated using 3D-Var technique to improve high resolution initial conditions. In order to evaluate the impact of the assimilation procedure at different horizontal resolutions and to assess the impact of assimilating reflectivity data from multiple radars, several experiments using Weather Research and Forecasting (WRF) model are performed. Finally, traditional verification scores as accuracy, equitable threat score, false alarm ratio and frequency bias, interpreted analyzing their uncertainty through bootstrap confidence intervals (CIs), are used to objectively compare the experiments, using rain gauge data as benchmark.

**Keywords:** radar data assimilation, WRF, 3D-Var, MET, bootstrap confidence intervals, HyMeX

## 1 Introduction

In the last few years, a large number of floods caused by different meteorological events occurred in Italy. These events mainly affected small areas (few hundreds of square kilometers) making their forecast very difficult. Indeed, one of the

36 most important factors in producing a flash flood was found to be the persistence of the meteorological system over the  
37 same area in the presence of specific hydrological conditions (the size and the topography of the drainage basin, the  
38 amount of urban use within the basin, and so on), allowing for accumulating large amount of rain (Doswell et al., 1996).  
39 In complex orography areas, such the Italian regions, this is largely due to the barrier effect produced by the mountains,  
40 such as the Apennines. Moreover, the Mediterranean basin is affected by a complex meteorology, due to the peculiar  
41 distribution of land and water and to the Mediterranean Sea temperature, which is warmer than that of the European  
42 northern seas (Baltic Sea and North Sea). These factors may produce severe meteorological events: for example, if  
43 precipitation persists over urbanized watersheds with steep slopes, devastating floods can occur in a relatively short  
44 time.

45 The scientific community widely recognizes the need of numerical weather prediction (NWP) models to be run at high  
46 resolution for improving very short term quantitative precipitation forecasts (QPF) during severe weather events and  
47 flash floods. The combination of NWP models and weather radar observations has shown improved skill with respect to  
48 extrapolation-based techniques (Sun et al., 2014). Nevertheless, the accuracy of the mesoscale NWP models is  
49 negatively affected by the “spin-up” effect (Daley 1991) and is mostly dependent on the errors in the initial and lateral  
50 boundary conditions (IC and BC, respectively), along with deficiencies in the numerical models themselves, and at the  
51 resolution of kilometers even more critical because of the lack of high resolution observations, beside for radar data.  
52 Several studies in the meteorological field have demonstrated that the assimilation of appropriate data into the NWP  
53 models, especially radar (Sugimoto et al., 2009) and satellite ones (Sokol, 2009), significantly reduces the “spin-up”  
54 effect and improves the IC and BC of the mesoscale models. Classical observations such as TEMP (upper level  
55 temperature, humidity, and winds observations) or SYNOP (surface synoptic observations) do not have enough density  
56 to describe for example local convection, while radar measurements can provide a sufficient density of data. Maiello et  
57 al. (2014) showed the positive effect of the assimilation of radar data into the precipitation forecast of a heavy rainfall  
58 event occurred in central Italy. The authors showed the gain by using assimilating radar data with respect to the  
59 conventional ones. Similar results are obtained for a case of severe convective storm in Croatia by Stanesic and  
60 Brewster (2016).

61 Weather radar has a fundamental role in showing tridimensional structures of convective storms and the associated  
62 mesoscale and microscale systems (Nakatani, 2015). As an example, Xiao and Sun (2007) showed that the assimilation  
63 of radar observation at high resolution (2 km) can improve convective systems prediction. Recent researches in  
64 meteorology have established that the assimilation of real-time data, especially radar measurements (radial velocities  
65 and/or reflectivities), into the mesoscale NWP models can improve predicted precipitations for the next few hours. (e.g.  
66 Xiao et al., 2005; Sokol and Rezacova, 2006; Dixon et al., 2009; Salonen et al., 2010).

67 The aim of this study is to investigate the potential of improving NWP rainfall forecasts by assimilating multiple radar  
68 reflectivity data in combination or not with conventional observations. This may have a direct benefit also for  
69 hydrological applications, particularly for real time flash flood prediction and consequently for civil protection  
70 purposes. Major obstacles, that makes the assimilation of radar reflectivities into NWP models a challenging problem  
71 both mathematically and physically, lie in the non-linear relation between radar reflectivity and precipitation intensity  
72 as well as in the rapid evolution of mesoscale systems. While radial velocities observation operator is linear and based  
73 directly on prognostic model variables (i.e. wind), the assimilation of radar reflectivity is more challenging than radial  
74 velocity, because the observation operator of radar reflectivity is highly non-linear and has a non-Gaussian error  
75 probability density function.

The novelty of the paper is in exploring the impact on the high-resolution forecast of the assimilation of multiple radar reflectivity data in a complex orography area, such as central Italian regions, to predict intense precipitation. This aim is reached by using the IOP4 of the SOP1 in the framework of the HyMeX campaign (Ducrocq et al. 2014, Ferretti et al. 2014, Davolio et al. 2015). The SOP1 was held from 5 September to 5 November 2012; the IOP4 was issued for the central Italy target area on 14 September 2012 and it was tagged both as a Heavy Precipitation Event (HPE) and a Flash Flood Event (FFE). The reflectivity measured by three C-band weather radars was ingested together with traditional meteorological observations (SYNOP and TEMP) using 3D-Var to improve WRF model performance. So far, several studies about reflectivity data assimilation in heavy rainfall cases have been performed (e.g. Ha et al. 2011, Das et al. 2015) also including multiple radars data and in complex orography (e.g. Lee et al. 2010, Liu et al. 2013). However, this is the first experiment conducted on the Italian territory taking advantage of the reflectivity data collected by all the radars that cover central Italy.

The manuscript is arranged as follows. Section 2 provides information on the flash flood event and WRF model configuration. Section 3 presents the observations to be assimilated, the WRF 3D-Var data assimilation system, and the evaluation method used. The results are showed and assessed in the fourth and fifth Section. Summary and conclusions are reflected in the last Section.

## **2 Study area and model set up**

Flash floods are still one of the natural hazards producing human and economic losses (Llasat et al. 2013). Moreover, an increasing trend of the occurrence of severe events in the whole Mediterranean area has been found by several authors (Hertig et al. 2012, Martin et al. 2013, Diodato and Bellocchi, 2014). These open issues drove the HyMeX programme (<http://www.hymex.org>) aims at a better understanding of the water cycle in the Mediterranean with focus on extreme weather events. The observation strategy of HyMeX is organized in a long-term (4 years) Enhanced Observation Periods (EOP) and short-term (2 months) Special Observation Periods (SOP). During the SOP1, that was held from 5 September to 5 November 2012 with the major aim of investigating still-unclear mesoscale meteorological mechanisms over the Mediterranean area, three Italian hydro-meteorological sites were identified within the Western Mediterranean Target Area (TA): Liguria–Tuscany (LT), northeastern Italy (NEI) and central Italy (CI). Several Intensive Observing Periods (IOPs) were issued during the campaign to document Heavy Precipitation Events (HPE), Flash Floods Events (FFE) and Orographic Precipitation Events (ORP).

### **2.1 Case study**

During the day of 14 September 2012 a deep upper level trough entered the Mediterranean basin and deepened over the Tyrrhenian Sea slowly moving south eastward. A cut-off low developed over central Italy (Figure 1a, c) advecting cold air along the central Adriatic coast producing instability over central and southern Italy, and enhanced the Bora flow over the northern Adriatic Sea. Convection with heavy precipitations occurred in the morning of September 14 mainly along the central eastern Italian coast (Marche and Abruzzo regions), associated with the cut-off low over the Tyrrhenian Sea, producing flood in the urban area of Pescara (central western coast of Abruzzo region) where rainfall reached 150 mm in a few hours causing several river overflows, a landslide and many damages in the area of the city hospital. Progressive motion south-eastward of the cut-off and its filling (Figure 1b, d) gradually moved phenomena over south of Italy, even if some instability still remained over medium Adriatic until the afternoon of Saturday

115 September 15. At the same time, a ridge developed high pressure on the west part of West Mediterranean domain; this  
116 ridge slowly drifts eastwards during the weekend.

117 Figure 2, produced using DEWETRA operational platform, shows the interpolated map of 24h accumulated rainfall  
118 recorded from rain gauges network from September 14 to September 15 (00:00-00:00UTC) with a maximum  
119 accumulated rainfall on the highest peak of Abruzzo region (Campo Imperatore) approximately reaching 300 mm in 24  
120 hours. DEWETRA (Italian Civil Protection Department, CIMA Research Foundation, 2014) is an operational web  
121 platform used by the Italian Civil Protection Department (DPC) and implemented by CIMA Research Foundation  
122 (<http://www.cimafoundation.org/en/>). DEWETRA allows synthesis, integration and comparison of information  
123 necessary for instrumental monitoring, models forecasting and to build real-time risk scenarios and their possible  
124 evolution. Rain gauges time series of some selected stations in Marche and Abruzzo regions, where most significant  
125 amount of rainfall is accumulated are presented in Figure 3: Fermo and Pintura di Bolognola (Marche region)  
126 respectively with nearly 130 mm in 24h (Figure 3a) and 180 mm in 24h (Figure 3b); Campo Imperatore, Atri and  
127 Pescara Colli (Abruzzo region) with respectively nearly 300 mm (Figure 3c), 160 mm (Figure 3d) and 140 mm (Figure  
128 3e) in 24h. It is clearly shown (Figure 3) that the accumulation started around 02:00UTC of 14 September: in Fermo,  
129 Atri and Pescara Colli most of rainfall was concentrated in the first half of the day, whereas in Pintura di Bolognola and  
130 Campo Imperatore, precipitation fell all day long. The large amount of hourly precipitation for Atri and Pescara Colli  
131 respectively at 06:00UTC and 05:00UTC (red ovals in Fig. 3d and 3e) reaching 45mm/h, indicating convective  
132 precipitation, whereas rainfall at Campo Imperatore rain gauge (Fig. 3c) was much weaker but lasting longer which  
133 allowed for reaching an accumulated amount of approximately 300 mm in 24h.

134 Figure 4 shows the Vertical Maximum Intensity (VMI) reflectivity product from the Italian radar network (Vulpiani et  
135 al., 2008a) superimposed onto the Meteosat Second Generation (MSG) 10.8  $\mu\text{m}$  image (in normalized inverted  
136 greyscale). A zoom over the central Italy target area highlights a line of convective cells along the Apennines in central  
137 Italy due to the western flow approaching the orographic barrier. VMI values above 45 dBZ are associated with intense  
138 precipitation that occurred during convective events.

## 139 2.2 WRF model set up

140

141 The numerical weather prediction experiments are performed in this work using the non-hydrostatic Advanced  
142 Research WRF (ARW) modeling system V3.4.1. It is a primitive equations mesoscale meteorological model, with  
143 terrain-following vertical coordinates and options for different physical parameterizations. Skamarock et al. (2008)  
144 provides a detailed overview of the model.

145 In this study, a one-way nested configuration using the *ndown* program is used: a 12 km domain ( $263 \times 185$ ) that covers  
146 central Europe and west Mediterranean basin (referred as D01) is initialized using the European Centre for Medium-  
147 Range Weather Forecasts (ECMWF) analyses at 0.25 degrees of horizontal resolution; an innermost domain, that covers  
148 the whole Italy (referred as D02), with a grid space of 3 km ( $445 \times 449$ ) using as BC and IC the output of the previous  
149 forecast at 12 km. Both domains run with 37 unequally spaced vertical levels, from the surface up to 100 hPa (Figure  
150 5).

151 Taking into account that the performance of a mesoscale model is highly related to the parameterization schemes, the  
152 main physics packages used in this study are set as for the operational configuration (Ferretti et al., 2014) used at the

153 centre of Excellence CETEMPS (<http://cetemps.aquila.infn.it/>). They include (Skamarock et al., 2008): the “New”  
154 Thompson et al. 2004 microphysics scheme, the MYJ (Mellor-Yamada-Janjic) scheme for the PBL (planetary boundary  
155 layer), the Goddard shortwave radiation scheme and the RRTM (rapid radiative transfer model) longwave radiation  
156 scheme, the Eta similarity scheme for surface layer formulation and the Noah LSM (Land Surface Model) to  
157 parameterize physics of land surface. A few preliminary tests are performed to assess the best cumulus parameterization  
158 scheme to be used both for the coarse and finest resolution domain for this event. Hence, the following  
159 parameterizations are tested: the new Kain–Fritsch and the Grell 3D schemes. The latter is an enhanced Dudhia of the  
160 Grell-Deveneyi scheme, in our simulations only used on the lowest resolution domain, where the option *cugd\_avedx*  
161 (subsidence spreading) is switched on. Based on the results of these two cumulus parameterization schemes, the one  
162 producing the best precipitation forecast will be used to evaluate the impact of data assimilation.

163

### 164 **3 Data and methodology**

165

166 This section will be focused on the description of types of observations ingested into the assimilation procedure, namely  
167 both conventional and radar, and on the 3D-Var methodology as well as the observation operator used for the  
168 calculation of the reflectivity. Moreover, a brief overview of the evaluation method adopted to assess the performance  
169 of numerical weather predictions will be given.

170

#### 171 **3.1 Observations to be assimilated**

172 Conventional observations SYNOP and TEMP were retrieved from the ECMWF Meteorological Archival and Retrieval  
173 System (MARS). They have been packed in a suitable format for ingest into the assimilation procedure using the  
174 Observation Preprocessor (OBSPROC) module provided by the 3D-Var system. Among its main functions there are  
175 also to perform a quality control check and to assign observational errors based on a pre-specified error file. In short, a  
176 total of 983 observations (967 SYNOP and 16 TEMP) are ingested into the coarse resolution domain, whereas a total of  
177 338 (333 SYNOP and 5 TEMP) observations into the high resolution one.

178 Reflectivities taken from three C-band Doppler radars operational during the IOP4 have been assimilated to improve IC.  
179 The radars have different technical characteristics and were operated with different scanning strategies and operational  
180 settings as shown in Table 1: each radar has a half power beam width of 1.6, 1 and 0.9 degree respectively for Monte  
181 Midia (MM), Polar55C (P55C) and San Pietro Capofiume (SPC) and a range resolution of 500, 75 and 250 metres.

182 MM and SPC radars are included in the Italian weather radar network, while P55C radar is a research radar working on  
183 demand, but **it** was operational during the IOPs of the HyMeX campaign (Roberto et al., 2016).

184 It is worth mentioning that radar data can be affected by numerous sources of errors, mainly due to ground clutter,  
185 attenuation due to propagation or beam blocking, anomalous propagation and radio interferences. This is the reason  
186 why a preliminary "cleaning" procedure is applied to the measured radar reflectivity from the three radars before the  
187 assimilation process, consisting of the following 3 steps:

- 188 • a first quality check of radar volumes to filter out radar pixels affected by ground clutter and anomalous  
189 propagation. Furthermore, Z was corrected for attenuation using a methodology based on the specific  
190 differential phase shift ( $K_{dp}$ ) available for dual polarization radars (Vulpiani et al, 2015); moreover, reflectivity

is not corrected for partial beam blocking: all the data that are affected by partial beam blocking and clutter have been filtered out;

- volume reflectivity radar data are converted from their native polar coordinates (range, azimuth and altitude) into geographical Cartesian ones (latitude, longitude and altitude);

- the minimum assimilated reflectivity is set to -20 dBZ.

Moreover, no observation thinning is performed because this procedure is not yet developed into the 3D-Var system for radar data. Instead, an iterative approach has been applied to extract more information from radar data during the assimilation procedure: this is the multiple outer loops technique explained later in Section 4.

### 3.2 3D-Var data assimilation method

Data assimilation (DA) is a technique employed in many fields of geosciences perhaps most importantly in weather forecasting and hydrology. In this context it is the procedure by which observations are combined with the product (*first guess* or *background forecast*) of a NWP model and their corresponding error statistics, to produce a bettered estimate (the *analysis*) of the true state of the atmosphere (Skamarock et al., 2008). The variational DA method realizes this through the iterative minimization of a penalty function (Ide et al., 1997):

$$J(\mathbf{x}) = J^b(\mathbf{x}) + J^o(\mathbf{x}) = \frac{1}{2} \{ [\mathbf{y}^0 - H(\mathbf{x})]^T \mathbf{R}^{-1} [\mathbf{y}^0 - H(\mathbf{x})] + (\mathbf{x} - \mathbf{x}^b)^T \mathbf{B}^{-1} (\mathbf{x} - \mathbf{x}^b) \}, \quad (1)$$

where  $\mathbf{x}^b$  is the first guess state vector,  $\mathbf{y}^0$  is the assimilated observation vector,  $H$  is the observation operator that links the model variables to the observation variables and  $\mathbf{x}$  is the unknown analysis state vector to be found by minimizing  $J(\mathbf{x})$ . Finally,  $\mathbf{B}$  and  $\mathbf{R}$  are the background covariance error matrix and the observation covariance error matrix, respectively.

The minimization of the penalty function  $J(\mathbf{x})$ , displayed by Equation (1), is the a posteriori maximum likelihood estimate of the true atmosphere state, given the two sources of a priori data that are  $\mathbf{x}^b$  and  $\mathbf{y}^0$  (Lorenc, 1986).

In this study the 3D-Var system developed by Barker et al. (2003, 2004) is used for assimilating radar reflectivity and conventional observations SYNOP and TEMP. The penalty function minimization is performed in a preconditioned control variable space, where the preconditioned control variables are pseudo relative humidity, stream function, unbalanced temperature, unbalanced potential velocity and unbalanced surface pressure. Because of radar reflectivity assimilation is considered, the total water mixing ratio  $q_t$  is chosen as the moisture control variable. The following equation presents the observation operator used by the 3D-Var to calculate reflectivity for the comparison with the observed one (Sun and Crook, 1997):

$$Z = 43.1 + 17.5 \log(\rho q_r), \quad (2)$$

where  $\rho$  and  $q_r$  are the air density in  $\text{kg/m}^3$  and the rainwater mixing ratio in  $\text{g/kg}$ , respectively, while  $Z$  is the co-polar radar reflectivity factor expressed in dBZ. Since the total water mixing ratio  $q_t$  is used as the control variable, a warm rain process (Dudhia, 1989) is introduced into the WRF-3D-Var system to allow for producing the increments of moist variables linked to the hydrometeors.

229 The performance of the DA system strongly depends on the quality of the  $\mathbf{B}$  matrix in Equation (1). In this study, a  
 230 specific background error statistics is computed for both domains for the entire SOP1 duration using the National  
 231 Meteorological Center (NMC) method (Parrish and Derber, 1992). This technique estimates the initial state error using  
 232 differences of couples of forecasts valid at the same time, but with one of them having a delayed start time. One of the  
 233 advantage of this method is that it maintains information on the dynamic of the model itself, but it may not give the  
 234 proper correlation structure on data-sparse observations. Commonly, for regional applications and to remove the diurnal  
 235 cycle, a delay of 24 hours between the forecasts (T+24 minus T+12) is used; nevertheless, this delay can produce  
 236 overestimated correlation length scales compared to those needed by a variational data assimilation technique, because  
 237 of too dynamically evolved structures (Sadiki et al., 2000). Since 3D-Var is applied to the Mediterranean area,  $\mathbf{B}$  has to  
 238 take into account the scale of the motions of this orographic and meteorologically complex area: the model grid  
 239 resolution ranges between 12 km and 3 km, therefore the errors have to describe the physical phenomena relative to  
 240 these scales.

241

### 242 3.3 Evaluation

243

244 The Point-Stat Tool of MET (Model Evaluation Tools) application (DTC, 2013), developed at the DTC (Developmental  
 245 Testbed Center, NCAR), has been used to objectively evaluate the 12 hours accumulated precipitation produced by  
 246 WRF on both domains. The interpolation method used to match the gridded model output to the point observation is the  
 247 distance weighted mean in a 3 x 3 square of grid points. The observations used for the statistical evaluation were  
 248 obtained from the DEWETRA platform of the Department of Civil Protection and the comparison has been performed  
 249 over central Italy target area using about 3000 rain gauges with a good coverage throughout the Italian territory.  
 250 Moreover, for interpreting results from the verification analysis bootstrap, confidence intervals (CIs) have been used to  
 251 analyze the uncertainty associated with the score's values. Bootstrapping is a non parametric, computationally  
 252 expensive, statistical technique (Efron & Tibshirani, 1993) for estimating parameters and uncertainty information, that  
 253 allows to make inferences from data without making strong distributional assumptions about the data or the statistic  
 254 being calculated. Therefore, the idea was to estimate CIs to set some bounds (bootstrap upper and lower confidence  
 255 limits) on the expected value of the verification score helping to assess whether differences between competing  
 256 forecasts are significant.

257

## 258 4 Design of the numerical experiments: discussion of the results

259

260 The simulations on the coarser resolution domain (D01) are run from 12:00UTC of 13 September 2012 and integrated  
 261 for the following 96 hours, whereas runs on the finest resolution domain (D02) started at 00:00UTC of September 14  
 262 for a total of 48 hours of integration. The previous coarser resolution WRF forecast at 00:00UTC is used as the first  
 263 guess in the 3D-Var experiment, because 00:00UTC has been selected as the "*analysis time*" of the assimilation  
 264 procedure. After assimilation, the lateral and lower boundary conditions are updated for the high resolution forecast.  
 265 Finally, the new IC and BC are used for the model initialization (in a warm start regime) at 00:00UTC. As already  
 266 pointed out a set of preliminary experiments are performed using different cumulus convective scheme to assess the  
 267 best one to be used. The following experiments are performed without assimilation and using the convective scheme on



the coarser resolution domain only: KAIN-FRITSCH (KF\_MYJ); GRELL3D (GRELL3D\_MYJ); GRELL3D associated with the CUGD factor (GRELL3D\_MYJ\_CUGD). The best performance is obtained by Grell3D scheme which is able to simulate the peak of precipitation cumulated in 24h over Campo Imperatore, whereas KAIN-FRITSCH completely misses it (not shown here). The MET statistical analysis support the previous finding and the simulation with *cugd\_avedx* activated shows a significant performance in terms of uncertainty of the calculated scores than the other two simulations (not shown). Here after GRELL3D\_MYJ\_CUGD is referred as the control experiment (CTL) performed without any data assimilation.

At this point analysis of a new set of simulations is performed allowing to establish the best model configuration for the radar reflectivity assimilation. The DA experiments aim to investigate:

1. the impact of the assimilation at low and high resolution by assimilating both conventional and non-conventional data at both resolutions;
2. the impact of the assimilation of different types of observations;
3. the impact of the different radars, which is investigated by performing experiment by assimilating conventional data and then adding radar one by one.

Therefore in Table 2, together with CTL simulation, the following DA experiments are summarized: i) the assimilation of conventional data only (CON); ii) the assimilation of reflectivity data from MM only (CONMM) are added; iii) the assimilation of P55C radar reflectivity is added to the previous experiments (CONMMPOL); iv) the assimilation of the third radar reflectivity data is added to the previous (CONMMPOLSPC). Finally, an experiment to assess the role of the outer loops is performed (CONMMPOLSPC3OL): to include non-linearities into the observation operator and to evaluate the impact of reflectivity data entering for each cycle, the multiple outer loops strategy is applied (Hsiao et al. 2012). According to this approach, the non-linear problem is solved iteratively as a progression of linear problems: the assimilation system is able to ingest more observations by running more than one analysis outer loop, allowing observations rejected in the previous loop to be enter into the subsequent one. Since radar data are non linearly related to the analysis control variables, the outer loops method is particularly helpful to extract more information from such data. For example, over a total amount of 518400 radar data (considering all the three radars), the fraction of radar observations assimilated into the 3 km domain at the first outer iteration is 32986, at the second outer iteration is 33001 and at the last one is 33027.

In the following section the results will be presented and discussed following the rationale of the previously introduced experiments and analyzing the uncertainty (confidence level of 95%) in the realized scores (Forecast Accuracy (ACC), Frequency Bias (FBIAS), Equitable Threat Score (ETS), False Alarm Ratio (FAR)) for performance quantitative assessment.

## **5 Impact of conventional measurements and radar reflectivity assimilation on rainfall forecast: low versus high resolution**

In figure 6, a preliminary comparison among low resolution (LR) simulations is shown. The control simulation (CTL) without data assimilation is shown in Figure 6a; whereas the other panels (b, c, d, e, f) show the experiments performed using the data assimilation.



304 The outputs of different experiments in Fig. 6 have been eyeballed and we found that CONMMPOLSPC\_LR\_12KM  
 305 (black arrow in Fig. 6e) shows the most encouraging performance compared to the observed accumulated rainfall of  
 306 Figure 2: the rainfall maximum over Campo Imperatore is very well simulated, however a slight cell displacement at the  
 307 border between Marche and Abruzzo regions is noticeable. The rain cumulated by the gauges in 24h related to this cell  
 308 is around 300 mm (Fig. 3c); in the simulations shown in Figures 6b and 6f this cell is reproduced, although its position  
 309 is shifted in another region. Furthermore, the precipitation pattern along the northern coasts of Abruzzo (black oval in  
 310 Fig. 6e) is also quite well forecasted. At an objective comparison of the statistical indices (not shown here) with their  
 311 relative upper and lower confidence limits for the 12 hours accumulated precipitation and for two thresholds (1 mm and  
 312 40 mm for light and heavy rain regimes respectively), we obtained likely good values for ACC and FAR for all the  
 313 experiments and for heavy rain regimes, strengthened by a small uncertainty interval. On the other hand, for the lower  
 314 threshold the values of FBias for all simulations, considering also the confidence intervals, are greater than one. One  
 315 possible interpretation of the impact of the lower threshold is that with 95% confidence all the experiments are  
 316 overestimating the frequency of precipitation around 1 mm/12h.

317 Similarly to the above comparison, in figure 7 high resolution results (HR) obtained performing reflectivity assimilation  
 318 on 12 km domain (column 1), on 3 km (column 2) and on 12 km and 3 km together (column 3) are presented; to the top  
 319 of figure 7 the CTL experiment on D02 is shown. Figure 7 is organized as follows: viewing panels by line, on line 1 all  
 320 the simulations with conventional data assimilation only (CON\*) are found; on line 2 all the experiments with the  
 321 assimilation of the reflectivity data from MM radar added (CONMM\*); on line 3 all the experiments with the  
 322 assimilation of the reflectivity data from 2 C-band radars added (CONMMPOL\*); on line 4 all the experiments with the  
 323 assimilation of the reflectivity data from all 3 C-band radars added (CONMMPOLSPC\*); on line 5 the simulations  
 324 where the strategy of outer loops is adopted (CONMMPOLSPC3OL\*). In order to quantify the uncertainty associated to  
 325 these experiments, the bootstrap 95% confidence intervals for verification statistics ACC, FBias, ETS, FAR have been  
 326 summarized over tables (from 3 to 5) reporting the two thresholds of precipitation for light and heavy rain regimes: 1  
 327 mm/12h and 40 mm/12h, respectively.

328 In order to investigate the impact of the assimilation at different resolutions, we examine figure 7 by column and  
 329 comparing it with the available observations (Fig. 2) using also the statistical analysis:

- 330 • column 1 (12KM): CTL produces an overestimation of the rainfall that is not corrected by the assimilation of  
 331 conventional data, but assimilating the reflectivity from the 3 radars (column 1 line 4) and also introducing the  
 332 3 outer loops (column 1 line 5) the main cells are better reproduced. MET indices (not shown here) suggest  
 333 that CTL and CON\_HR\_12KM have the largest difference between the CIs bounds for higher thresholds of  
 334 FBias: this result suggests that the remaining simulations, with smallest difference in CIs limits and with both  
 335 bounds lower than 1, surely underestimate the frequency of heavy precipitating events. Another aspect to point  
 336 out is that some indices for all simulations are quite close to each other and within the CIs, so it is not possible  
 337 to discern which is the best experiment over all;
- 338 • column 2 (3KM): a partial correction of the rainfall overestimation compared to column 1 is observed  
 339 especially if reflectivity from all the radars are assimilated together with conventional data and the outer loops  
 340 strategy is applied (column 2 line 5); the statistical indices in Table 3 show as the most competitive experiment  
 341 among the assimilated ones the CONMMPOLSPC3OL\_3KM for lower threshold of rain for ACC (0.83) and

FBIAS (0.96), on the other hand CONMM\_3KM is the most promising simulation for heavy rain threshold for the indices FBIAS (0.31) and ETS (0.13);

- column 3 (12KM\_3KM): rainfall overestimation was partially corrected compared to columns 1 and 2 by all experiments; the MET statistics in Table 3 shows that CTL and CONMMPOLSPC3OL\_12KM\_3KM are the experiments with encouraging values and small uncertainty for ACC and ETS especially for light rain regimes, although there is a quite broad spread in FBIAS for CTL experiment (score 0.47, with a lower and upper CIs limit of respectively 0.14 and 1.61) if we consider higher thresholds.

The frequency of rainfall underestimation for higher thresholds found in the mother domain when radar reflectivity data are assimilated in D01 only has been reduced by switching to a higher resolution domain, moreover, the overestimation of the frequency for lower thresholds has been corrected because the FBIAS, previously systematically above 1 is found approximately 1 (indices not shown). Furthermore, general improvements (especially for FBIAS and ETS) come out for heavy rain regimes when radar reflectivity assimilation has been performed on the highest resolution domain, whereas the ingestion of conventional observations produces the worst results for FBIAS and ETS since a smaller number of them were assimilated into the finest resolution domain (for instance one sounding on five total) than that the coarser one. Data assimilation, operated on both 12 km and 3 km, shows similar performances to the experiments where assimilation is performed only on D01, but a worse response for higher thresholds (Table 3) than the ones where assimilation is carried out on D02.

In order to examine the impact of the assimilation of different data and radars, we can now analyze the experiments showed in figure 7 line by line. The results are compared with the observations of Fig. 2. The following considerations are worth discussing:

- line 1 (CON): a strong reduction of the rainfall is found with respect to CTL if conventional data are assimilated, but the rainfall pattern remains unchanged. Statistical indices of CON experiment (Table 4) do not improve the performances of CTL (despite a reduction in some cases of the spread between the CIs limits for higher thresholds of the FBIAS). Some indices values suggest a slightly better performance when the conventional observations are assimilated only on the bigger domain and for higher thresholds (FBIAS 0.49), together with an improvement of FAR index for heavy rain regime (FAR 0.001);
- line 2 (CONMM): a further reduction in the precipitation overestimation is found as well as some variations in the pattern of the rainfall; the scores in Table 4, together with their bootstrap upper and lower limits, show that MM radar reflectivity and conventional observations assimilation, improves the model performance above all for lower thresholds respect to the experiments where only SYNOP and TEMP were ingested. It applies also for some of the scores at higher thresholds (for example for ETS);
- line 3 (CONMMPOL): a quite strong improvement in the rainfall amount is found for all simulations. However, from the statistics of Table 4, we found a general worsening of the results both for light and heavy rain regimes when POL is added (especially for FBIAS and ETS, in some cases also for ACC and FAR at lower thresholds);
- line 4 (CONMMPOLSPC): a clear correction of the rainfall pattern is found; the overestimation produced by the simulation where the reflectivity from all the radars are assimilated on the 3 km domain has been corrected by the experiment in which the reflectivity is assimilated both on D01 and D02; the uncertainty in the realized

scores of Table 4 suggests that the addition of SPC radar improves the results, furthermore they are not better than those where only MM is ingested;

- line 5 (CONMMPOLSPC3OL): the outer loops experiment confirms the strong overestimation reduction by \*12KM\_3KM; from Table 5 it seems that the introduction of 3OL improves the indices estimate and bounds above all when the 12 km domain is considered (see FBIAS and ETS for both rain regimes and FAR for lower thresholds).

In summary, simulations results show that assimilation of conventional data is better to perform on the lowest resolution domain because more observations were used in the coarser domain, whereas when the assimilation is performed on the highest resolution domain only few SYNOP and even less TEMP fell down in the 3 km domain at the analysis time of the assimilation procedure. The impact of conventional observations are expected to be lower than those of non conventional ones, because most of them have already been used by ECMWF to produce their analysis and that they are here used as first guess, even if at lower resolution (0.25°). Therefore, they result to be correlated to the background and the improvements of those experiments where they are assimilated are expected to be low.

With regard to the assimilation of reflectivity radar data, it should be noted that P55C radar observations of the event considered is shielded at the lowest elevation angles by the Apennines range and provides a limited contribution to reflectivity data that are assimilated. Also the outer loops strategy could have an important role in the assimilation procedure, but this latter needs a further investigation (for example an additional work has to be dedicated to testing the different tuning factors for both observation and background during each outer loop) because a general rainfall underestimation for higher thresholds is found.

The results of this section confirm that when there is a correlation between the observations and the first guess used, the results of the data assimilation are poor, especially if no "special" observation is available on a wide area. The assimilation of a large amount of surface data together with the radiosonde ones decreases the quality of the final analysis produced. It probably depends on the different density of the surface and the three dimensional data of radiosondes, as assessed by Liu and Rabier (2002), being the former much larger than the latter.

## 6 Conclusions

In this manuscript the effects of multiple radar reflectivity data assimilation on a heavy precipitation event occurred during the SOP1 of the HyMeX campaign have been evaluated: the aim is to build a regionally-tuned numerical prediction model and decision-support system for environmental civil protection services within the central Italian regions. A sensitivity study at different domain resolution and using different types of data to improve initial conditions has been performed by assimilating into the WRF model radar reflectivity measurements, collected by three C-band Doppler weather radars operational during the event that hit central Italy on 14 September 2012. 3D-Var and MET are the WRF tools used to assess this purpose. The study is performed on the complex basin, both for the orography and physical phenomena, of the Mediterranean area. First of all, WRF model responses to different types of cumulus parameterizations have been tested to establish the best configuration and to obtain the control simulation. The latter has been compared with observations and other experiments performed using 3D-Var. The set of assimilation experiments have been conducted following two different strategies: i) data assimilation at low and high resolution or at both

417 resolutions simultaneously; ii) conventional data against radar reflectivity data assimilation. Both have been examined  
418 to assess the impact on rainfall forecast.

419 The major findings of this work have been the following:

- 420 • Grell 3D parameterization improves the simulations both on D01 and D02 and the use of the spreading factor is  
421 an added value in properly predict heavy rainfall over inland of Abruzzo and the rainfall pattern along the  
422 northeast coast;
- 423 • investigating the impact of the assimilation at different resolutions, positive results are showed by the  
424 experiments where the data assimilation is performed on both domains 12 km and 3 km;
- 425 • the impact of the assimilation using different types of observations shows improvements if reflectivity from all  
426 the radars, along with SYNOP and TEMP are assimilated; furthermore, MM is the one that gives more  
427 optimistic results due to its excellent monitoring of the whole event;
- 428 • the outer loops strategy allows for further improving positive impact of the assimilation of multiple reflectivity  
429 radars data. Moreover, a deeper investigation of this approach is required to well assess its impact, above all  
430 concerning the running time in an operational context;
- 431 • we have seen that there are thresholds where the WRF 3D-Var is statistically significant, with 95% confidence,  
432 while for other thresholds we have to be careful in drawing conclusions above all in the face of large  
433 uncertainty or when the score values are quite close to each other.

434 From the results obtained in this study, it is not possible to assess, in general terms, which is the best model  
435 configuration. In fact, this analysis should be performed systematically with a significant number of flash flood case  
436 studies before one can claim with certainty the positive impact of multiple reflectivity radar observations assimilation  
437 upon the forecast skill. Nevertheless, this work has pointed out aspects in 3D-Var reflectivity data assimilation that  
438 encourages to investigate more flash flood events occurred over central Italy, in order to make the proposed approach  
439 suitable to provide a realistic prediction of possible flash floods both for the timing and localization of such events. To  
440 confirm and consolidate these initial findings, apart from analyzing more case studies, a deeper analysis of the  
441 meteorology of the region and of the performance of the data assimilation system throughout longer trials in a "pseudo-  
442 operational" procedure is necessary. Moreover, a more sophisticated spatial verification technique (MODE, Method for  
443 Object-Based Diagnostic Evaluation, Davis et al., 2006a, 2006b) which focuses on the realism of the forecast, by  
444 comparing features or 'objects' that characterize both forecast and observation fields, could be investigated in the  
445 future. In fact, spatial verification methods are particularly suitable to address the model capability to reproduce  
446 structures like the convective systems responsible for the high precipitation events as considered in the present research,  
447 which, because of their typical dimensions, need high resolution simulations to be predicted (Gilleland et al., 2009).  
448 These new-generation spatial verification methods, through the identification and the geometrical description of  
449 'objects' in forecast and observation fields (e.g. accumulated precipitation or radar reflectivity), permit an evaluation of  
450 the forecast skill in a more consistent way.

451

## 452 **Acknowledgements**

453 We are grateful to the Gran Sasso National Laboratories for support in computing resources, as well as the National  
454 Civil Protection Department and CIMA Research Foundation for rain gauges data using for the model validation.

455 NCAR is also acknowledged for WRF model, 3D-Var system and MET tool. This work aims at contributing to the  
456 HyMeX programme.

457

## 458 **References**

459

460 Barker, D.M., Huang, W., Guo, Y.-G., and Bourgeois, A.: A Three-Dimensional Variational (3D-Var) Data  
461 Assimilation System For Use With MM5. NCAR Tech. Note, NCAR/TN-453+STR, UCAR Communications, Boulder,  
462 CO, 68pp, 2003.

463 Barker, D.M., Huang, W., Guo, Y.-R., Bourgeois, A., and Xiao, Q.: A Three-Dimensional Variational (3D-Var) Data  
464 Assimilation System For Use With MM5: Implementation and Initial Results. *Mon. Wea. Rev.*, 132, 897-914, 2004.

465 Daley, R.: Atmospheric Data Analysis, Cambridge University Press, Cambridge, UK, 1991.

466 Das, M. K., M. A. M. Chowdhury, S. Das, S. K. Debsarma, and S. Karmakar: Assimilation of Doppler weather radar  
467 data and their impacts on the simulation of squall events during premonsoon season. *Natural Hazards*, 77(2), 901–931.  
468 DOI: 10.1007/s11069-015-1634-9, 2015.

469 Davis A. C., Brown B., Bullock R.: Object-Based verification of precipitation forecasts. Part I: methodology and  
470 application to mesoscale rain areas. *Mon. Wea. Rev.* 134, 1772-1784, 2006a.

471 Davis A. C., Brown B., Bullock R.: Object-Based verification of precipitation forecasts. Part II: application to  
472 convective rain system. *Mon. Wea. Rev.* 134, 1785-1795, 2006b.

473 Davolio, S., Ferretti, R., Baldini, L., Casaioli, M., Cimini, D., Ferrario, M. E., Gentile, S., Loglisci, N., Maiello, I.,  
474 Manzato, A., Mariani, S., Marsigli, C., Marzano, F. S., Miglietta, M. M., Montani, A., Panegrossi, G., Pasi, F., Pichelli,  
475 E., Pucillo, A. and Zinzi, A.: The role of the Italian scientific community in the first HyMeX SOP: an outstanding  
476 multidisciplinary experience. *Meteorologische Zeitschrift*, 24, 261-267, 2015.

477 Developmental Testbed Center, 2013: MET: Version 4.1 Model Evaluation Tools Users Guide. Available at  
478 <http://www.dtcenter.org/met/users/docs/overview.php>. 226 pp.

479 Diodato N. and Bellocchi G. (eds.), Storminess and Environmental Change, Advances in Natural and Technological  
480 Hazards Research 39, DOI 10.1007/978-94-007-7948-8\_2, *Springer Science+Business Media Dordrecht* 2014.

481 Dixon, M., Li, Z., Lean, H., Roberts, N., and Ballard, S.: Impact of data assimilation on forecasting convection over the  
482 United Kingdom using a high-resolution version of the Met Office Unified Model, *Mon. Weather Rev.*, 137, 1562–  
483 1584, 2009.

484 Doswell C.A III., Brooks A.E., and Maddox R.A.: Flash Flood Forecasting: An Ingredients-Based Methodology.  
485 *Weather and Forecasting*, VOL. 11, 560-581, 1996.

486 Ducrocq, V., Braud, I., Davolio, S., Ferretti, R., Flamant, C., Jansà, A., Kalthoff, N., Richard, E., Taupier-Letage, I.,  
487 Ayral, P.-A., Belamari, S., Berne, A., Borga, M., Boudevillain, B., Bock, O., Boichard, J.-L., Bouin, M.-N., Bousquet,  
488 O., Bouvier, C., Chiggiato, J., Cimini, D., Corsmeier, U., Coppola, L., Cocquerez, P., Defer, E., Delanoë, J., Di  
489 Girolamo, P., Doerenbecher, A., Drobinski, P., Dufournet, Y., Fourrié, N., Gourley, J. J., Labatut, L., Lambert, D., Le  
490 Coz, J., Marzano, F. S., Molinié, G., Montani, A., Nord, G., Nuret, M., Ramage, K., Rison, B., Roussot, O., Said, F.,

491 Schwarzenboeck, A., Testor, P., Van-Baelen, J., Vincendon, B., Aran, M. and Tamayo, J.,: HyMeX-SOP1, the field  
 492 campaign dedicated to heavy precipitation and flash flooding in the northwestern Mediterranean. *Bulletin of the*  
 493 *American Meteorological Society*, **95**, 1083-1100, 2014.

494 Dudhia, J.: Numerical study of convection observed during the winter monsoon experiment using a mesoscale two-  
 495 dimensional model, *J. Atmos. Sci.*, 46, 3077–3107, 1989.

496 Efron, B. & R. J. Tibshirani: *An Introduction to the Bootstrap*. New York: Chapman and Hall, 1993.

497 Ferretti, R., E. Pichelli, S. Gentile, I. Maiello, D. Cimini, S. Davolio, M. M. Miglietta, G. Panegrossi, L. Baldini, F.  
 498 Pasi, F. S. Marzano, A. Zinzi, S. Mariani, M. Casaioli, G. Bartolini, N. Loglisci, A. Montani, C. Marsigli, A. Manzato, A.  
 499 Pucillo, M. E. Ferrario, V. Colaiuda, and R. Rotunno: Overview of the first HyMeX Special Observation Period over  
 500 Italy: observations and model results. *Hydr. Earth Syst. Sci.*, 18, 1953-1977, 2014, doi:10.5194/hess-18-1953-2014,  
 501 2014.

502 Gilleland, E., Ahijevych, D., Brown, B.G., Casati, B., Ebert, E.E.: Intercomparison of spatial forecast verification  
 503 methods. *Weather Forecast.* 24, 1416–1430, 2009.

504 Ha, J.-H., H.-W. Kim, and D.-K. Lee: Observation and numerical simulations with radar and surface data assimilation  
 505 for heavy rainfall over central Korea. *Advances in Atmospheric Sciences*, 28(3), 573–590. DOI: 10.1007/s00376-  
 506 0100035-y, 2011.

507 Hertig E., Paxian A., Vogt G., Seubert S., Paeth H., Jacobeit J.: Statistical and dynamical downscaling assessments of  
 508 precipitation extremes in the Mediterranean area. *Meteorologische Zeitschrift*, Vol. 21 No. 1 , p. 61 - 77, 2012.

509 Hsiao L.-F., Chen D.-S., Kuo Y.-H., Guo Y.-R., Yeh T.-C., Hong J.-S. and Fong C.-T.: Application of WRF 3DVAR to  
 510 Operational Typhoon Prediction in Taiwan: Impact of Outer Loop and Partial Cycling Approaches. *Wea. Forecasting*  
 511 27.5, pp. 1249–1263. issn: 1520-0434. doi: 10.1175/waf-d-11-00131.1. url: [http://dx.doi.org/10.1175/WAF-D11-](http://dx.doi.org/10.1175/WAF-D11-00131.1)  
 512 00131.1, 2012.

513 Ide, K., Courtier, P., Ghil, M., and Lorenc, A. C.: Unified notation for data assimilation: Operational, sequential and  
 514 variational, *J. Meteorol. Soc. Jpn.*, 75, 181–189, 1997.

515 Italian Civil Protection Department and CIMA Research Foundation: *The Dewetra Platform: A Multi-perspective*  
 516 *Architecture for Risk Management during Emergencies*. Springer International Publishing Switzerland, Chapter  
 517 *Information Systems for Crisis Response and Management in Mediterranean Countries*, Volume 196 of the  
 518 series *Lecture Notes in Business Information Processing* pp 165-177, 2014. DOI 10.1007/978-3-319-11818-5\_15

519 Llasat, M. C., Llasat-Botija, M., Petrucci, O., Pasqua, A. A., Rosselló, J., Vinet, F., and Boissier, L.: Towards a  
 520 database on societal impact of Mediterranean floods within the framework of the HYMEX project, *Nat. Hazards Earth*  
 521 *Syst. Sci.*, 13, 1337-1350, doi:10.5194/nhess-13-1337-2013, 2013.

522 Lee, J.-H., H.-H. Lee, Y. Choi, H.-W. Kim, and D.-K. Lee: Radar data assimilation for the simulation of mesoscale  
 523 convective systems. *Advances in Atmospheric Sciences*, 27(5), 1025–1042. DOI: 10.1007/s00376-010-9162-8, 2010.

524 Liu Z.-Q. and Rabier F.: The interaction between model resolution, observations resolution and observations density in  
 525 data assimilation: a one-dimensional study. *Quart. J. Roy. Meteor. Soc.*, 128, 1367-1386, 2002.

526 Liu, J., M. Bray, and D. Han: A study on WRF radar data assimilation for hydrological rainfall prediction. *Hydrology*  
527 *and Earth System Sciences*, 17(8), 3095– 3110. DOI: 10.5194/hess-17-3095-2013, 2013.

528 Lorenc, A. C.: Analysis methods for numerical weather prediction, *Q. J. Roy. Meteorol. Soc.*, 112, 1177–1194, 1986.

529 Maiello, I., Ferretti, R., Gentile, S., Montopoli, M., Picciotti, E., Marzano, F. S., and Faccani, C.: Impact of radar data  
530 assimilation for the simulation of a heavy rainfall case in central Italy using WRF–3DVAR, *Atmos. Meas. Tech.*, 7,  
531 2919-2935, doi:10.5194/amt-7-2919-2014, 2014.

532 Martín J. R., García M. M., Dávila F. de P., Soriano L. R.: Severe rainfall events over the western Mediterranean Sea: A  
533 case study. *Atmospheric Research*, 127, 47–63, 2013.

534 Nakatani T., Misumi R., Shoji Y., Saito K., Seko H., Seino N., Suzuki S-I., Shusse Y., Maesaka T., and Sugawara H. ;  
535 Tokyo metropolitan area convection study for extreme weather resilient cities. *BAMS*, 96, ES123-ES126, 2015.

536 Parrish, D.F. and Derber, J.C.: The National Meteorological Center’s Spectral Statistical-Interpolation Analysis System.  
537 *Mon. Wea. Rev.*, 120, 1747-1763, 1992.

538 Roberto, N., Adirosi, E., Baldini, L., Casella, D., Dietrich, S., Gatlin, P., Panegrossi, G., Petracca, M., Sanò, P., and  
539 Tokay, A.: Multi-sensor analysis of convective activity in central Italy during the HyMeX SOP 1.1, *Atmos. Meas.*  
540 *Tech.*, 9, 535-552, doi:10.5194/amt-9-535-2016, 2016.

541 Sadiki W., Fischer C. and Geleyn J.-F.: Mesoscale Background Error Covariances: Recent Results Obtained with the  
542 Limited-Area Model ALADIN over Morocco. *Mon. Wea. Rev.*, 128, 3927-3935, 2000.

543 Salonen K, Haase G, Eresmaa R, Hohti H, Järvinen H.: Towards the operational use of Doppler Radar radial winds in  
544 HIRLAM. *Atmospheric Research* 100: 190–200, 2010.

545 Skamarock, W.C., Klemp, J.B., Dudhia, J., Gill, D.O., Barker, D.M., Duda, M. G., Huang, X.-Y., Wang, W., and  
546 Powers, J. G.: A description of the Advanced Research WRF Version 3. NCAR Technical Note. TN 475+STR, 113  
547 pp., available from [www.mmm.ucar.edu/wrf/users/docs/arw\\_v3.pdf](http://www.mmm.ucar.edu/wrf/users/docs/arw_v3.pdf) (last access: January 2012), 2008.

548 Sokol, Z. and Rezacova, D.: Assimilation of Radar reflectivity into the LMCOSMO model with a high horizontal  
549 resolution, *Meteorol. Appl.*, 13, 317–330, 2006.

550 Sokol, Z.: Effects of an assimilation of Radar and satellite data on a very short range forecast of heavy convective  
551 rainfalls, *Atmos. Res.*, 93, 188–206, 2009.

552 Stanesic A., and K.A. Brewster: Impact of Radar Data Assimilation on the Numerical Simulation of a Severe Storm in  
553 Croatia. *Met.Zeit.* Vol. 25, No. 1, 37–53, 2016

554 Sugimoto, S., Crook N.A., Sun J., Xiao Q., and Barker D.M.: An examination of WRF 3D-VarRadar data assimilation  
555 on its capability in retrieving unobserved variables and forecasting precipitation through observing system simulation  
556 experiments. *Mon. Wea. Rev.*, 137, 4011-4029, 2009. DOI:10.1175/2009MWR2839.1.

557 Sun, J. Xue, M., Wilson J. W., Zawadzki I., Ballard S.P., Onville-Hoimeyer J., Joe P., Barker D.M., Li P-W., Golding  
558 B., Xu M., and Pinto J.: Use of NWP for nowcasting convective precipitation, recent progress and challenges. *BAMS*,  
559 95, 409-426, 2014.



560 Sun, J. and Crook, N.A.: Dynamical and Microphysical Retrieval from Doppler RADAR Observations Using a Cloud  
561 Model and Its Adjoint. Part I: Model Development and Simulated Data Experiments. *J. Atmos. Sci.*, 54, 1642-1661,  
562 1997.

563 Thompson, G., R. M. Rasmussen, and K. Manning: Explicit forecasts of winter precipitation using an improved bulk  
564 microphysics scheme. Part I: Description and sensitivity analysis. *Mon. Wea. Rev.*, 132, 519–542, 2004.

565 Vulpiani G., Pagliara, P., Negri, M., Rossi, L., Gioia, A., Giordano, P., Alberoni, P. P., Cremonini, R., Ferraris, L., and  
566 Marzano, F. S.: The Italian radar network within the national early-warning system for multi-risks management, Proc.  
567 of Fifth European Conference on Radar in Meteorology and Hydrology (ERAD 2008), 184, Finnish Meteorological  
568 Institute, Helsinki, 30 June-4 July, 2008a.

569 Vulpiani, G., Baldini, L., and Roberto, N.: Characterization of Mediterranean hail-bearing storms using an operational  
570 polarimetric X-band radar, *Atmos. Meas. Tech.*, 8, 4681-4698, doi:10.5194/amt-8-4681-2015, 2015.

571 Xiao, Q., Kuo, Y.-H., Sun, J. and Lee, W.-C.: Assimilation of Doppler RADAR Observations with a Regional 3D-Var  
572 System: Impact of Doppler Velocities on Forecasts of a Heavy Rainfall Case. *J. Appl. Meteor.*, 44, 768-788, 2005.

573 Xiao, Q. and Sun, J.: Multiple-RADAR Data Assimilation and Short-Range Quantitative Precipitation Forecasting of a  
574 Squall Line Observed during IHOP\_2002. *Mon. Wea. Rev.*, 135, 3381-3404, 2007.

575  
576  
577

LIST OF FIGURES

578  
579  
580

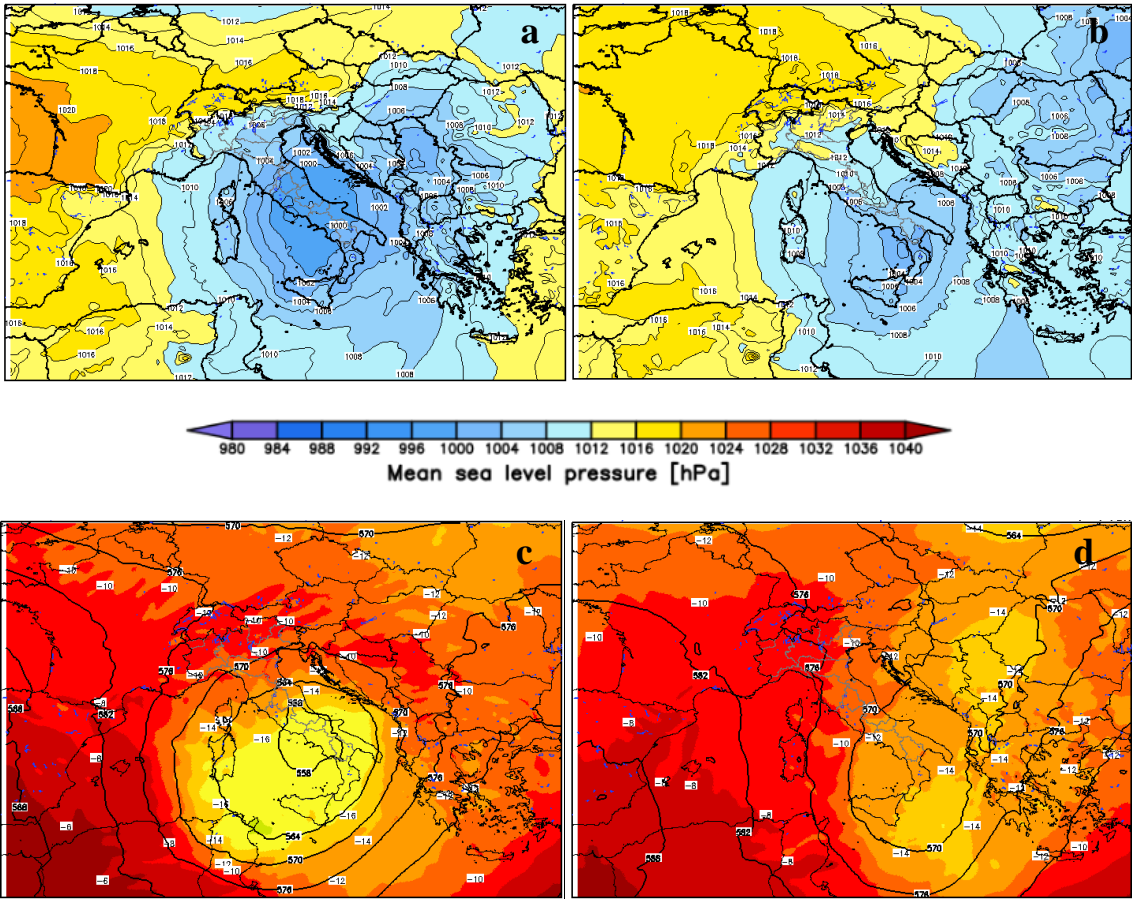




Figure 1. ECMWF (European Center for Medium-Range Weather Forecasts) analyses at 12:00UTC on 14 September 2012: a) mean sea level pressure, c) temperature (color shades) and geopotential height (black isolines) at 500 hPa; ECMWF analyses at 12:00UTC on 15 September 2012: b) mean sea level pressure, d) temperature (black isolines) and geopotential height (color shades) at 500 hPa.

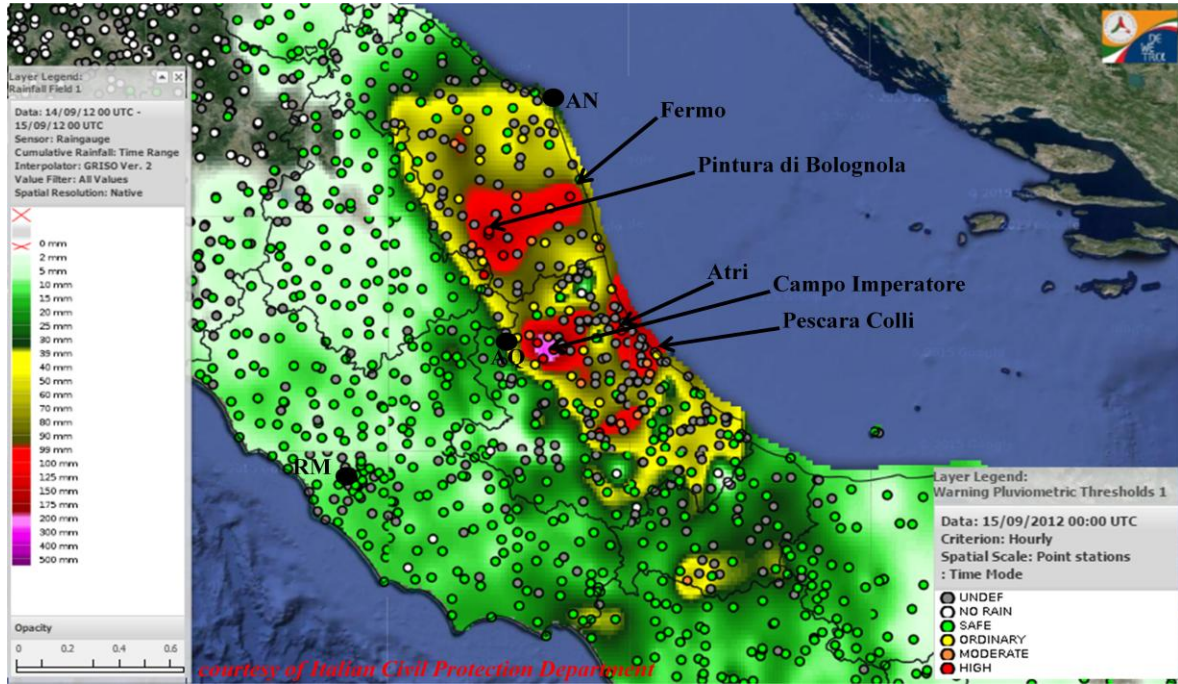
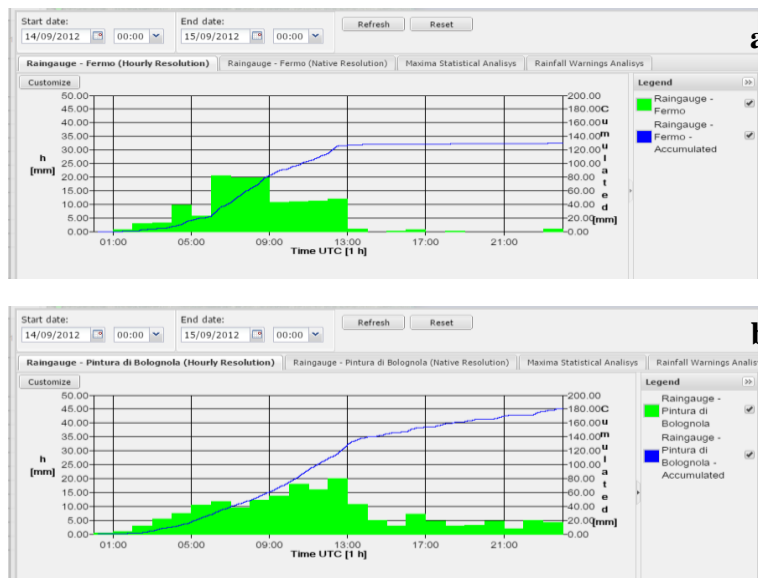


Figure 2: Interpolated map of 24h accumulated rainfall from 00:00UTC of 14 September 2012 over Abruzzo and Marche regions taken from DEWETRA system from rain gauges measurements. Black contours are the administrative boundaries of regions, while the colored circles represent the warning pluviometric thresholds.



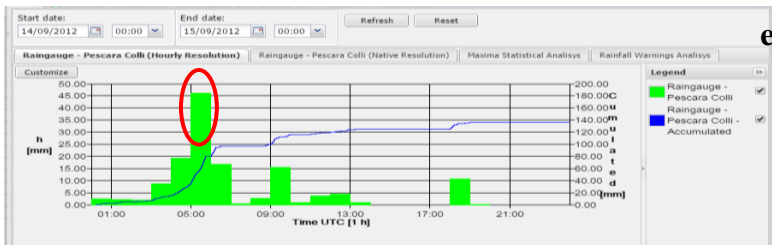
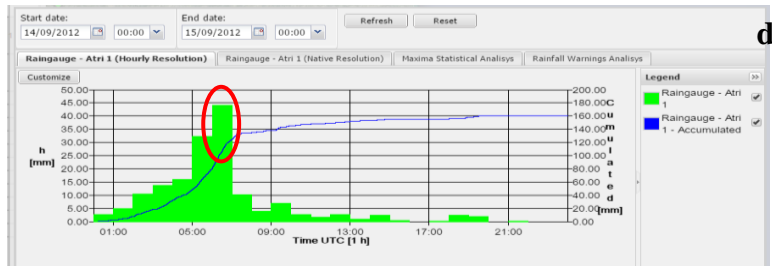
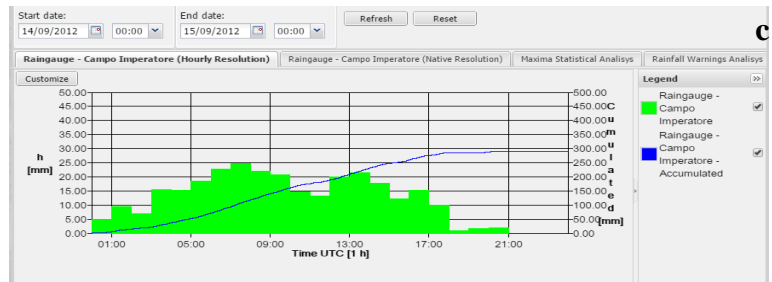


Figure 3: Rain gauges time series of some selected stations in Marche (a, Fermo and b, Pintura di Bolognola) and Abruzzo (c, Campo Imperatore, d, Atri and e, Pescara Colli) regions during the event of 14 September 2012. The green histogram represents the hourly accumulated precipitation (scale on the left); the blue line represents the incremental accumulation within the 24h (scale on the right). (courtesy of Italian Civil Protection Department)

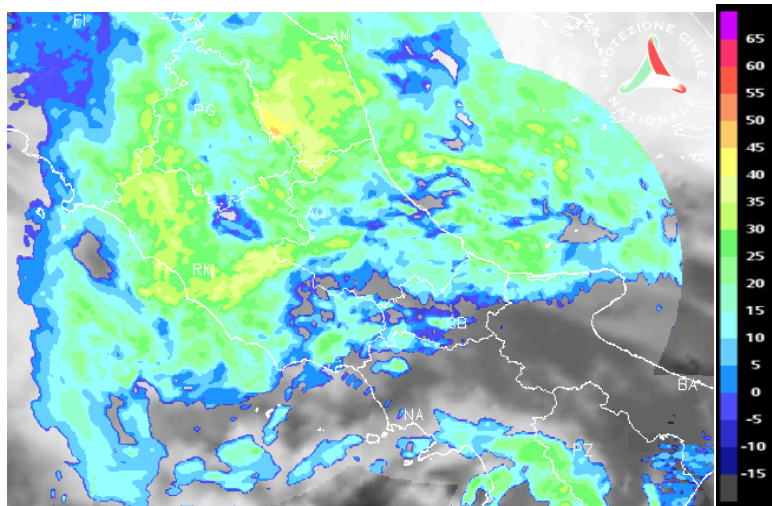


Figure 4: Zoom over central Italy of the reflectivity on 14 September 2012 at 08:00UTC from the Italian radar network overlapped with the MSG (IR 10.8) at 07:30UTC. (courtesy of Italian DPC)

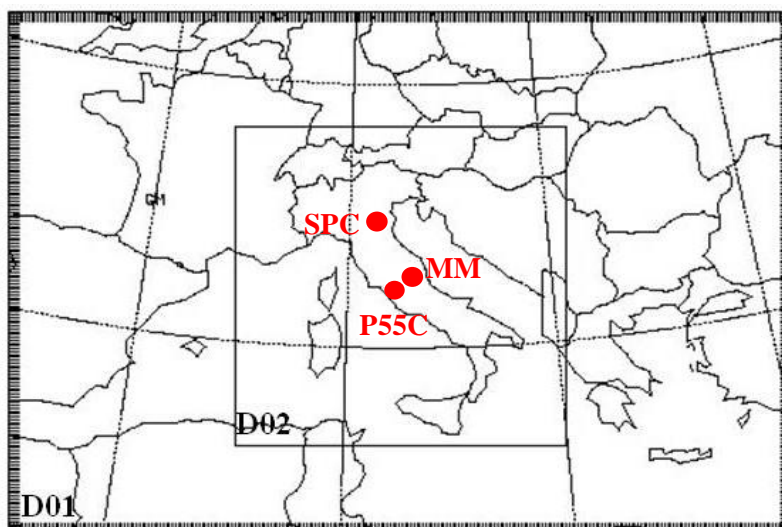
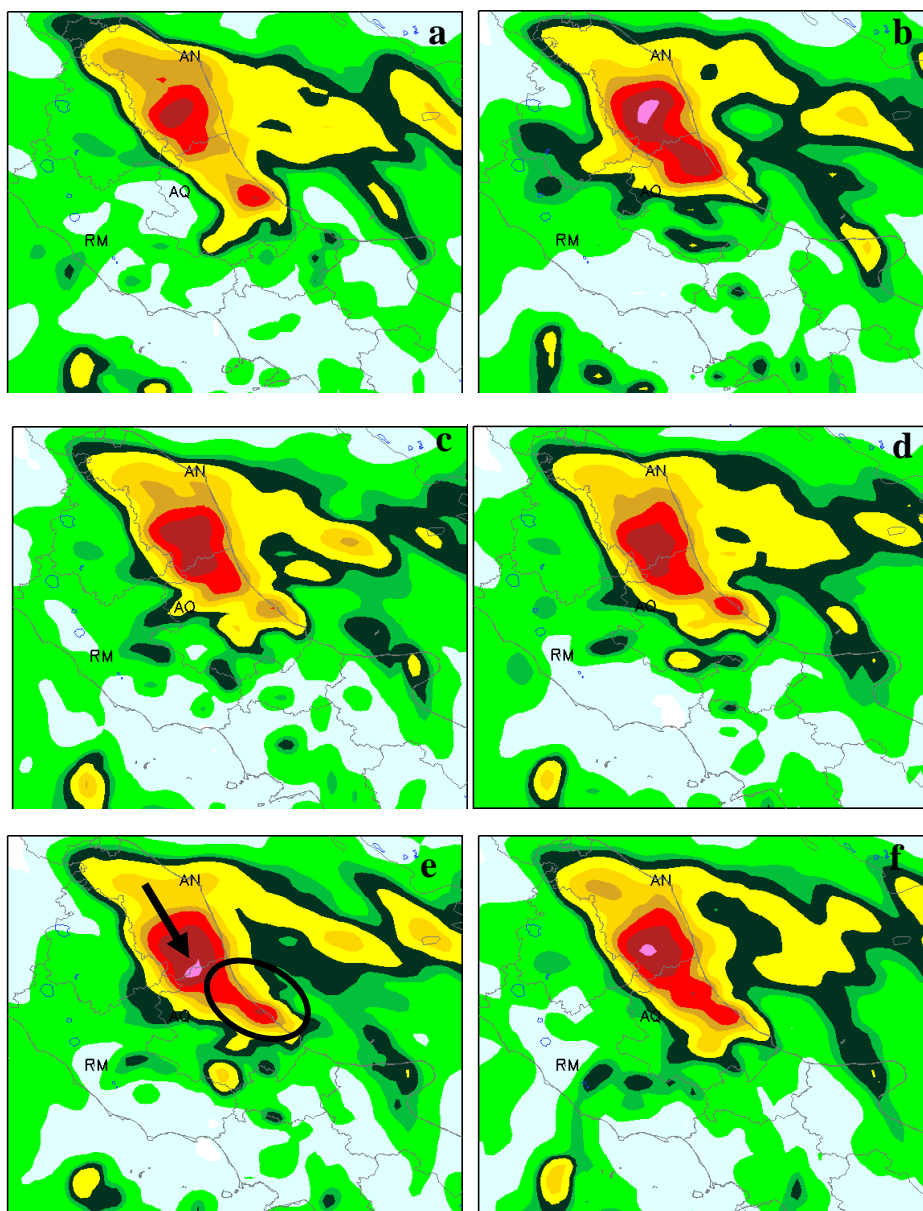


Figure 5: WRF *ndown* domains configuration: the two domains have respectively resolution of 12km and 3km. The high resolution D02 over Italy includes Mt. Midia (MM), ISAC-CNR (P55C) and San Pietro Capofiume (SPC) radars (red dots in the figure).





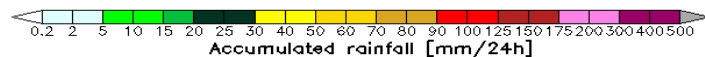
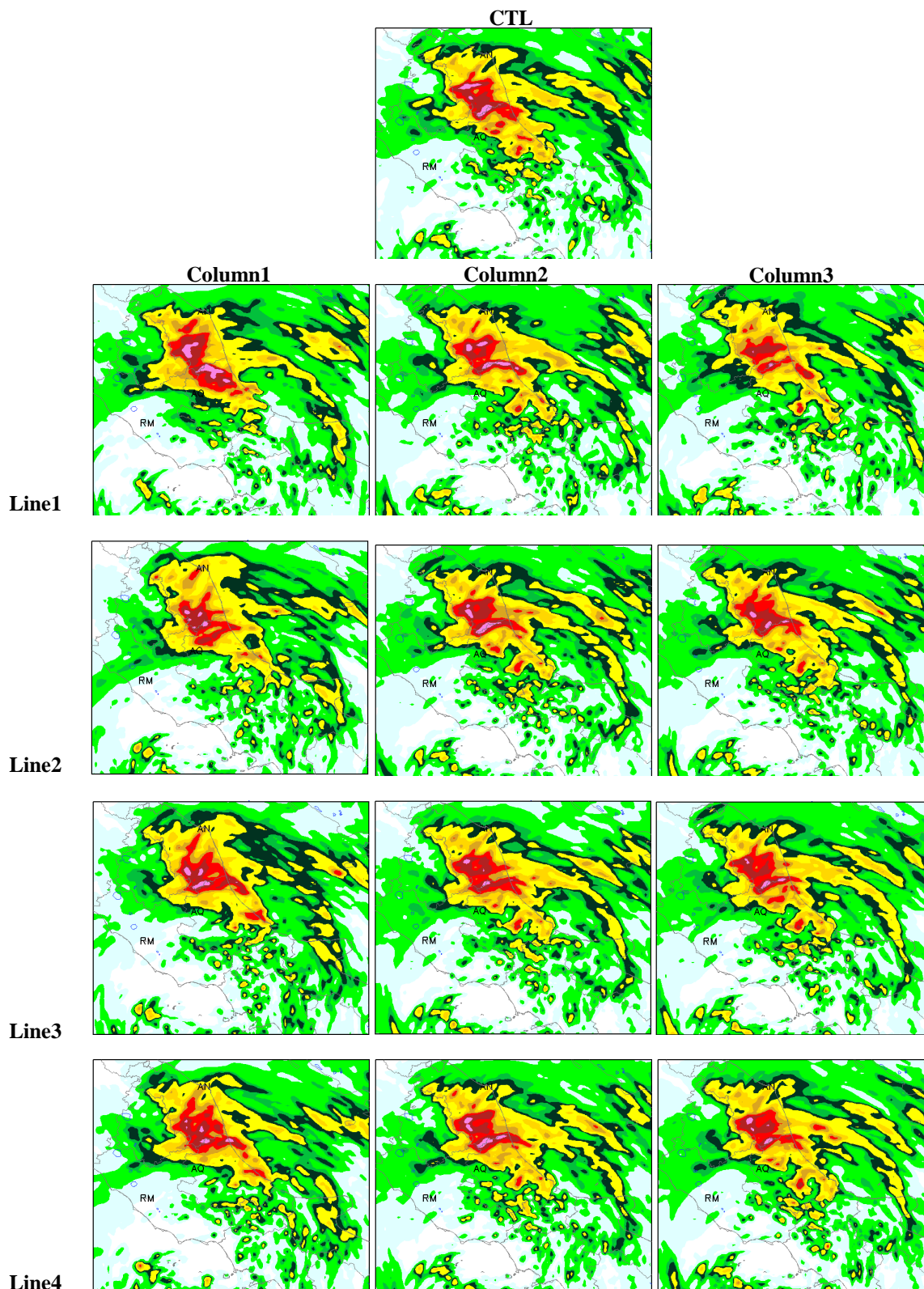


Figure 6: WRF D01 accumulated 24h rainfall forecast over central Italy from 00:00UTC of 14 September 2012: a) WRF D01 CTL; b) WRF D01 CON\_LR\_12KM; c) WRF D01 CONMM\_LR\_12KM; d) WRF D01 CONMMPOL\_LR\_12KM; e) WRF D01 CONMMPOLSPC\_LR\_12KM; f) WRF D01 CONMMPOLSPC3OL\_LR\_12KM.



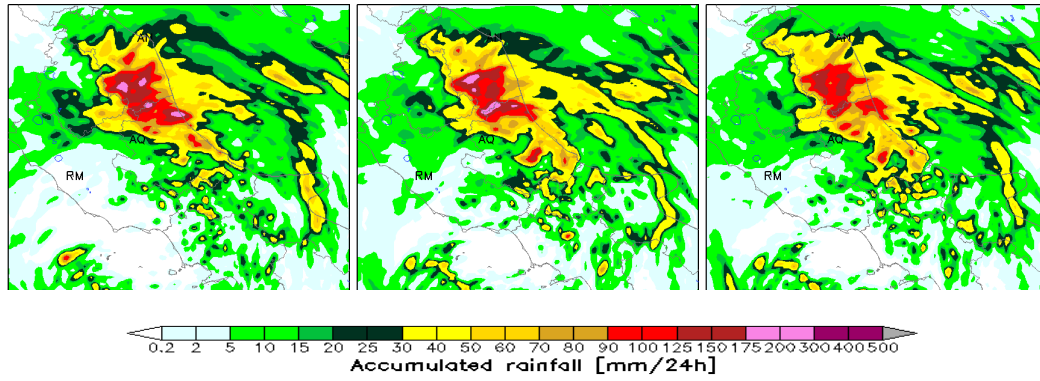


Figure 7: WRF D02 accumulated 24h rainfall forecast over central Italy from 00:00UTC of 14 September 2012: CTL simulation (top center); on each column simulations obtained performing reflectivity assimilation at different resolutions (\*12KM, \*3KM, \*12KM\_3KM); on each line simulations performed assimilating different kinds of data (CON\*, CONMM\*, CONMMPOL\*, CONMMPOLSPC\*, CONMMPOLSPC3OL\*).

Table 1: Technical characteristics of the three radars whose reflectivity have been assimilated during IOP4.

Features	Units	MM radar	P55C radar	SPC radar
Owner		CF Abruzzo Region	ISAC-CNR of Rome	Arpae Emilia Romagna
Location		Monte Midia	Rome	San Pietro Capofiume
Latitude	[deg]	42.057	41.840	44.6547
Longitude	[deg]	13.177	12.647	11.6236
Height (a.s.l.)	[m]	1760	131	31
Doppler		YES	YES	YES
Dual Polarization		NO	YES	YES
Range Resolution	[m]	500	75	250
Half Power Beam Width	[deg]	1.6	1	0.9
Temporal Resolution	[min]	15	5	15
Elevations angles used in PPI scans	[deg]	0, 1, 2, 3	0.6, 1.6, 2.6, 4.4, 6.2, 8.3, 11.0, 14.6	0.53, 1.4, 2.3, 3.2, 4.1, 5.0
Maximum Range	[km]	120 or 240	120	125

Table 2: List of experiments to test the impact of data assimilation.

Experiment	Cumulus	Grid Resolution	Assimilation Synop+Temp	Assimilation Radar
CTL	GRELL3D+CUGD	12KM/3KM	NO	NO
CON	GRELL3D+CUGD	12KM/3KM/BOTH	YES	NO
CONMM	GRELL3D+CUGD	12KM/3KM/BOTH	YES	MM

CONMMPOL	GRELL3D+CUGD	12KM/3KM/BOTH	YES	MM+POL
CONMMPOLSPC	GRELL3D+CUGD	12KM/3KM/BOTH	YES	MM+POL+SPC
CONMMPOLSPC3OL	GRELL3D+CUGD	12KM/3KM/BOTH	YES	MM+POL+SPC with 3 outer loops

636

637  
638  
639  
640  
641  
642

**Table 3: Bootstrap 95% confidence intervals for verification statistics Forecast Accuracy (ACC), Frequency Bias (FBIAS), Equitable Threat Score (ETS), False Alarm Ratio (FAR) and referred to experiments in column 2 and 3 respectively. They are considered as a function of thresholds (1mm/12h and 40mm/12h). The experiments are: CTL, CON\_3KM and CON\_12KM\_3KM, CONMM\_3KM and CONMM\_12KM\_3KM, CONMMPOL\_3KM and CONMMPOL\_12KM\_3KM, CONMMPOLSPC\_3KM and CONMMPOLSPC\_12KM\_3KM, CONMMPOLSPC3OL\_3KM and CONMMPOLSPC3OL\_12KM\_3KM.**

Experiment	ACC Thresholds mm/12h		FBIAS Thresholds mm/12h		ETS Thresholds mm/12h		FAR Thresholds mm/12h	
	1	40	1	40	1	40	1	40
CTL	(0.80) <b>0.83</b> (0.87)	(0.96) <b>0.98</b> (0.99)	(0.79) <b>0.94</b> (1.13)	(0.14) <b>0.47</b> (1.61)	(0.23) <b>0.33</b> (0.45)	(0.04) <b>0.10</b> (0.16)	(0.16) <b>0.21</b> (0.27)	(0.001) <b>0.007</b> (0.015)
CON_3KM	(0.78) <b>0.82</b> (0.85)	(0.96) <b>0.98</b> (0.99)	(0.65) <b>0.80</b> (0.98)	(0.08) <b>0.18</b> (0.42)	(0.14) <b>0.24</b> (0.35)	(0.03) <b>0.06</b> (0.12)	(0.17) <b>0.22</b> (0.28)	(0.001) <b>0.004</b> (0.009)
CON_12KM_3KM	(0.77) <b>0.81</b> (0.84)	(0.96) <b>0.98</b> (0.99)	(0.68) <b>0.84</b> (1.03)	(0.02) <b>0.10</b> (0.34)	(0.11) <b>0.20</b> (0.30)	(0.01) <b>0.04</b> (0.007)	(0.21) <b>0.27</b> (0.33)	(0) <b>0.001</b> (0.004)
CONMM_3KM	(0.78) <b>0.82</b> (0.86)	(0.97) <b>0.98</b> (0.99)	(0.79) <b>0.96</b> (1.17)	(0.14) <b>0.31</b> (0.68)	(0.17) <b>0.26</b> (0.37)	(0.05) <b>0.13</b> (0.26)	(0.18) <b>0.24</b> (0.29)	(0.001) <b>0.005</b> (0.11)
CONMM_12KM_3KM	(0.79) <b>0.83</b> (0.86)	(0.96) <b>0.98</b> (0.99)	(0.79) <b>0.96</b> (1.18)	(0.09) <b>0.31</b> (1.02)	(0.18) <b>0.28</b> (0.40)	(0.03) <b>0.07</b> (0.13)	(0.17) <b>0.23</b> (0.29)	(0.001) <b>0.006</b> (0.013)
CONMMPOL_3KM	(0.77) <b>0.81</b> (0.85)	(0.96) <b>0.98</b> (0.99)	(0.76) <b>0.94</b> (1.16)	(0.12) <b>0.28</b> (0.65)	(0.13) <b>0.23</b> (0.33)	(0.03) <b>0.09</b> (0.14)	(0.18) <b>0.24</b> (0.30)	(0.001) <b>0.006</b> (0.11)
CONMMPOL_12KM_3KM	(0.77) <b>0.81</b> (0.85)	(0.96) <b>0.98</b> (0.99)	(0.79) <b>0.96</b> (1.19)	(0.11) <b>0.26</b> (0.65)	(0.14) <b>0.23</b> (0.33)	(0.03) <b>0.08</b> (0.14)	(0.19) <b>0.25</b> (0.31)	(0.001) <b>0.006</b> (0.011)
CONMMPOLSPC_3KM	(0.78) <b>0.82</b> (0.86)	(0.96) <b>0.98</b> (0.99)	(0.85) <b>1.03</b> (1.25)	(0.10) <b>0.27</b> (0.83)	(0.18) <b>0.28</b> (0.39)	(0.03) <b>0.07</b> (0.13)	(0.19) <b>0.24</b> (0.31)	(0.001) <b>0.005</b> (0.012)
CONMMPOLSPC_12KM_3KM	(0.77) <b>0.81</b> (0.85)	(0.97) <b>0.98</b> (0.99)	(0.87) <b>1.04</b> (1.28)	(0.09) <b>0.25</b> (0.70)	(0.16) <b>0.26</b> (0.37)	(0.04) <b>0.08</b> (0.14)	(0.22) <b>0.28</b> (0.34)	(0) <b>0.004</b> (0.009)



CONMMPOLSPC3OL_3KM	(0.79) <b>0.83</b> (0.86)	(0.97) <b>0.98</b> (0.99)	(0.81) <b>0.96</b> (1.17)	(0.10) <b>0.24</b> (0.64)	(0.17) <b>0.27</b> (0.39)	(0.05) <b>0.12</b> (0.19)	(0.21) <b>0.27</b> (0.33)	(0.000) <b>0.003</b> (0.007)
	(0.79) <b>0.83</b> (0.86)	(0.97) <b>0.98</b> (0.99)	(0.82) <b>0.98</b> (1.18)	(0.08) <b>0.15</b> (0.24)	(0.19) <b>0.30</b> (0.41)	(0.05) <b>0.11</b> (0.18)	(0.19) <b>0.25</b> (0.31)	(0) <b>0.002</b> (0.003)

643

644

645

646

647

648

649

**Table 4: Bootstrap 95% confidence intervals for verification statistics Forecast Accuracy (ACC), Frequency Bias (FBIAS), Equitable Threat Score (ETS), False Alarm Ratio (FAR) and referred to experiments in line 1, 2, 3, 4. They are considered as a function of thresholds (1mm/12h and 40mm/12h). The experiments are: CTL, CON\_3KM/CONMM\_3KM/CONMMPOL\_3KM/CONMMPOLSPC\_3KM, CON\_HR\_12KM/CONMM\_HR\_12KM/CONMMPOL\_HR\_12KM/CONMMPOLSPC\_12KM, CON\_12KM\_3KM/CONMM\_12KM\_3KM/CONMMPOL\_12KM\_3KM/CONMMPOLSPC\_12KM\_3KM.**

Experiment	ACC Thresholds mm/12h		FBIAS Thresholds mm/12h		ETS Thresholds mm/12h		FAR Thresholds mm/12h	
	1	40	1	40	1	40	1	40
CTL	(0.80) <b>0.83</b> (0.87)	(0.96) <b>0.98</b> (0.99)	(0.79) <b>0.94</b> (1.13)	(0.14) <b>0.47</b> (1.61)	(0.23) <b>0.33</b> (0.45)	(0.04) <b>0.10</b> (0.16)	(0.16) <b>0.21</b> (0.27)	(0.001) <b>0.007</b> (0.014)
	(0.78) <b>0.82</b> (0.85)	(0.96) <b>0.98</b> (0.99)	(0.65) <b>0.80</b> (0.98)	(0.08) <b>0.18</b> (0.42)	(0.14) <b>0.24</b> (0.35)	(0.03) <b>0.06</b> (0.12)	(0.17) <b>0.22</b> (0.28)	(0.001) <b>0.004</b> (0.009)
	(0.78) <b>0.82</b> (0.86)	(0.97) <b>0.98</b> (0.99)	(0.79) <b>0.96</b> (1.17)	(0.14) <b>0.31</b> (0.68)	(0.17) <b>0.26</b> (0.37)	(0.05) <b>0.13</b> (0.26)	(0.18) <b>0.24</b> (0.29)	(0.001) <b>0.005</b> (0.011)
CON_3KM	(0.77) <b>0.81</b> (0.85)	(0.96) <b>0.98</b> (0.99)	(0.76) <b>0.94</b> (1.16)	(0.12) <b>0.28</b> (0.65)	(0.13) <b>0.23</b> (0.33)	(0.03) <b>0.09</b> (0.14)	(0.18) <b>0.24</b> (0.30)	(0.001) <b>0.006</b> (0.011)
	(0.78) <b>0.82</b> (0.86)	(0.96) <b>0.98</b> (0.99)	(0.85) <b>1.03</b> (1.25)	(0.10) <b>0.27</b> (0.83)	(0.18) <b>0.28</b> (0.39)	(0.03) <b>0.07</b> (0.13)	(0.19) <b>0.25</b> (0.31)	(0.001) <b>0.005</b> (0.012)
	(0.77) <b>0.81</b> (0.85)	(0.96) <b>0.98</b> (0.99)	(0.75) <b>0.91</b> (1.11)	(0.21) <b>0.49</b> (1.61)	(0.15) <b>0.25</b> (0.36)	(0.03) <b>0.07</b> (0.13)	(0.20) <b>0.26</b> (0.31)	(0.005) <b>0.0011</b> (0.19)
CON_HR_12KM	(0.78) <b>0.82</b> (0.86)	(0.97) <b>0.98</b> (0.99)	(0.79) <b>0.95</b> (1.16)	(0.15) <b>0.29</b> (0.64)	(0.18) <b>0.28</b> (0.39)	(0.07) <b>0.14</b> (0.21)	(0.19) <b>0.24</b> (0.31)	(0) <b>0.004</b> (0.008)
	(0.76) <b>0.80</b> (0.84)	(0.97) <b>0.98</b> (0.99)	(0.66) <b>0.82</b> (1.01)	(0.07) <b>0.14</b> (0.25)	(0.10) <b>0.20</b> (0.30)	(0.03) <b>0.006</b> (0.11)	(0.20) <b>0.25</b> (0.31)	(0.001) <b>0.003</b> (0.006)
	(0.78) <b>0.82</b> (0.86)	(0.96) <b>0.98</b> (0.99)	(0.71) <b>0.86</b> (1.05)	(0.08) <b>0.22</b> (0.59)	(0.17) <b>0.28</b> (0.39)	(0.02) <b>0.06</b> (0.12)	(0.16) <b>0.21</b> (0.27)	(0.001) <b>0.005</b> (0.11)
CONMM_3KM	(0.78) <b>0.82</b> (0.86)	(0.97) <b>0.98</b> (0.99)	(0.79) <b>0.95</b> (1.16)	(0.15) <b>0.29</b> (0.64)	(0.18) <b>0.28</b> (0.39)	(0.07) <b>0.14</b> (0.21)	(0.19) <b>0.24</b> (0.31)	(0) <b>0.004</b> (0.008)
	(0.76) <b>0.80</b> (0.84)	(0.97) <b>0.98</b> (0.99)	(0.66) <b>0.82</b> (1.01)	(0.07) <b>0.14</b> (0.25)	(0.10) <b>0.20</b> (0.30)	(0.03) <b>0.006</b> (0.11)	(0.20) <b>0.25</b> (0.31)	(0.001) <b>0.003</b> (0.006)
	(0.78) <b>0.82</b> (0.86)	(0.96) <b>0.98</b> (0.99)	(0.71) <b>0.86</b> (1.05)	(0.08) <b>0.22</b> (0.59)	(0.17) <b>0.28</b> (0.39)	(0.02) <b>0.06</b> (0.12)	(0.16) <b>0.21</b> (0.27)	(0.001) <b>0.005</b> (0.11)
CONMMPOL_3KM	(0.78) <b>0.82</b> (0.86)	(0.96) <b>0.98</b> (0.99)	(0.79) <b>0.95</b> (1.16)	(0.15) <b>0.29</b> (0.64)	(0.18) <b>0.28</b> (0.39)	(0.07) <b>0.14</b> (0.21)	(0.19) <b>0.24</b> (0.31)	(0) <b>0.004</b> (0.008)
	(0.76) <b>0.80</b> (0.84)	(0.97) <b>0.98</b> (0.99)	(0.66) <b>0.82</b> (1.01)	(0.07) <b>0.14</b> (0.25)	(0.10) <b>0.20</b> (0.30)	(0.03) <b>0.006</b> (0.11)	(0.20) <b>0.25</b> (0.31)	(0.001) <b>0.003</b> (0.006)
	(0.78) <b>0.82</b> (0.86)	(0.96) <b>0.98</b> (0.99)	(0.71) <b>0.86</b> (1.05)	(0.08) <b>0.22</b> (0.59)	(0.17) <b>0.28</b> (0.39)	(0.02) <b>0.06</b> (0.12)	(0.16) <b>0.21</b> (0.27)	(0.001) <b>0.005</b> (0.11)
CONMMPOLSPC_3KM	(0.78) <b>0.82</b> (0.86)	(0.96) <b>0.98</b> (0.99)	(0.79) <b>0.95</b> (1.16)	(0.15) <b>0.29</b> (0.64)	(0.18) <b>0.28</b> (0.39)	(0.07) <b>0.14</b> (0.21)	(0.19) <b>0.24</b> (0.31)	(0) <b>0.004</b> (0.008)
	(0.76) <b>0.80</b> (0.84)	(0.97) <b>0.98</b> (0.99)	(0.66) <b>0.82</b> (1.01)	(0.07) <b>0.14</b> (0.25)	(0.10) <b>0.20</b> (0.30)	(0.03) <b>0.006</b> (0.11)	(0.20) <b>0.25</b> (0.31)	(0.001) <b>0.003</b> (0.006)
	(0.78) <b>0.82</b> (0.86)	(0.96) <b>0.98</b> (0.99)	(0.71) <b>0.86</b> (1.05)	(0.08) <b>0.22</b> (0.59)	(0.17) <b>0.28</b> (0.39)	(0.02) <b>0.06</b> (0.12)	(0.16) <b>0.21</b> (0.27)	(0.001) <b>0.005</b> (0.11)
CONMM_HR_12KM	(0.78) <b>0.82</b> (0.86)	(0.96) <b>0.98</b> (0.99)	(0.79) <b>0.95</b> (1.16)	(0.15) <b>0.29</b> (0.64)	(0.18) <b>0.28</b> (0.39)	(0.07) <b>0.14</b> (0.21)	(0.19) <b>0.24</b> (0.31)	(0) <b>0.004</b> (0.008)
	(0.76) <b>0.80</b> (0.84)	(0.97) <b>0.98</b> (0.99)	(0.66) <b>0.82</b> (1.01)	(0.07) <b>0.14</b> (0.25)	(0.10) <b>0.20</b> (0.30)	(0.03) <b>0.006</b> (0.11)	(0.20) <b>0.25</b> (0.31)	(0.001) <b>0.003</b> (0.006)
	(0.78) <b>0.82</b> (0.86)	(0.96) <b>0.98</b> (0.99)	(0.71) <b>0.86</b> (1.05)	(0.08) <b>0.22</b> (0.59)	(0.17) <b>0.28</b> (0.39)	(0.02) <b>0.06</b> (0.12)	(0.16) <b>0.21</b> (0.27)	(0.001) <b>0.005</b> (0.11)
CONMMPOL_HR_12KM	(0.78) <b>0.82</b> (0.86)	(0.96) <b>0.98</b> (0.99)	(0.79) <b>0.95</b> (1.16)	(0.15) <b>0.29</b> (0.64)	(0.18) <b>0.28</b> (0.39)	(0.07) <b>0.14</b> (0.21)	(0.19) <b>0.24</b> (0.31)	(0) <b>0.004</b> (0.008)
	(0.76) <b>0.80</b> (0.84)	(0.97) <b>0.98</b> (0.99)	(0.66) <b>0.82</b> (1.01)	(0.07) <b>0.14</b> (0.25)	(0.10) <b>0.20</b> (0.30)	(0.03) <b>0.006</b> (0.11)	(0.20) <b>0.25</b> (0.31)	(0.001) <b>0.003</b> (0.006)
	(0.78) <b>0.82</b> (0.86)	(0.96) <b>0.98</b> (0.99)	(0.71) <b>0.86</b> (1.05)	(0.08) <b>0.22</b> (0.59)	(0.17) <b>0.28</b> (0.39)	(0.02) <b>0.06</b> (0.12)	(0.16) <b>0.21</b> (0.27)	(0.001) <b>0.005</b> (0.11)
CONMMPOLSPC_HR_12KM	(0.78) <b>0.82</b> (0.86)	(0.96) <b>0.98</b> (0.99)	(0.79) <b>0.95</b> (1.16)	(0.15) <b>0.29</b> (0.64)	(0.18) <b>0.28</b> (0.39)	(0.07) <b>0.14</b> (0.21)	(0.19) <b>0.24</b> (0.31)	(0) <b>0.004</b> (0.008)
	(0.76) <b>0.80</b> (0.84)	(0.97) <b>0.98</b> (0.99)	(0.66) <b>0.82</b> (1.01)	(0.07) <b>0.14</b> (0.25)	(0.10) <b>0.20</b> (0.30)	(0.03) <b>0.006</b> (0.11)	(0.20) <b>0.25</b> (0.31)	(0.001) <b>0.003</b> (0.006)
	(0.78) <b>0.82</b> (0.86)	(0.96) <b>0.98</b> (0.99)	(0.71) <b>0.86</b> (1.05)	(0.08) <b>0.22</b> (0.59)	(0.17) <b>0.28</b> (0.39)	(0.02) <b>0.06</b> (0.12)	(0.16) <b>0.21</b> (0.27)	(0.001) <b>0.005</b> (0.11)

CON_12KM_3KM	(0.77) <b>0.81</b> (0.84)	(0.96) <b>0.98</b> (0.99)	(0.68) <b>0.84</b> (1.03)	(0.02) <b>0.10</b> (0.34)	(0.11) <b>0.20</b> (0.30)	(0.01) <b>0.04</b> (0.07)	(0.21) <b>0.27</b> (0.33)	(0) <b>0.001</b> (0.004)
CONMM_12KM_3KM	(0.79) <b>0.83</b> (0.86)	(0.96) <b>0.98</b> (0.99)	(0.79) <b>0.96</b> (1.18)	(0.09) <b>0.31</b> (1.01)	(0.18) <b>0.28</b> (0.40)	(0.03) <b>0.07</b> (0.13)	(0.17) <b>0.23</b> (0.29)	(0.001) <b>0.006</b> (0.013)
CONMMPOL_12KM_3KM	(0.77) <b>0.81</b> (0.85)	(0.96) <b>0.98</b> (0.99)	(0.79) <b>0.96</b> (1.19)	(0.11) <b>0.26</b> (0.65)	(0.14) <b>0.23</b> (0.33)	(0.03) <b>0.08</b> (0.13)	(0.19) <b>0.25</b> (0.31)	(0.01) <b>0.005</b> (0.011)
CONMMPOLSPC_12KM_3KM	(0.77) <b>0.81</b> (0.85)	(0.96) <b>0.98</b> (0.99)	(0.87) <b>1.04</b> (1.28)	(0.09) <b>0.25</b> (0.70)	(0.16) <b>0.26</b> (0.36)	(0.04) <b>0.08</b> (0.14)	(0.22) <b>0.28</b> (0.34)	(0) <b>0.004</b> (0.009)

**Table 5:** Bootstrap 95% confidence intervals for verification statistics Forecast Accuracy (ACC), Frequency Bias (FBIAS), Equitable Threat Score (ETS), False Alarm Ratio (FAR) and referred to experiments in line 5. They are considered as a function of thresholds (1mm/12h and 40mm/12h). The experiments are: CTL, CONMMPOLSPC3OL\_3KM, CONMMPOLSPC3OL\_HR\_12KM, CONMMPOLSPC3OL\_12KM\_3KM.

Experiment	ACC Thresholds mm/12h		FBIAS Thresholds mm/12h		ETS Thresholds mm/12h		FAR Thresholds mm/12h	
	1	40	1	40	1	40	1	40
CTL	(0.79) <b>0.83</b> (0.87)	(0.96) <b>0.98</b> (0.99)	(0.79) <b>0.94</b> (1.13)	(0.14) <b>0.47</b> (1.61)	(0.23) <b>0.33</b> (0.44)	(0.04) <b>0.10</b> (0.16)	(0.16) <b>0.21</b> (0.27)	(0.001) <b>0.007</b> (0.015)
CONMMPOLSPC3OL_3KM	(0.79) <b>0.83</b> (0.86)	(0.97) <b>0.98</b> (0.99)	(0.81) <b>0.96</b> (1.17)	(0.10) <b>0.24</b> (0.64)	(0.17) <b>0.27</b> (0.39)	(0.05) <b>0.12</b> (0.19)	(0.21) <b>0.27</b> (0.33)	(0) <b>0.003</b> (0.007)
CONMMPOLSPC3OL_HR_12KM	(0.78) <b>0.82</b> (0.86)	(0.96) <b>0.98</b> (0.99)	(0.77) <b>0.93</b> (1.13)	(0.13) <b>0.31</b> (0.86)	(0.20) <b>0.30</b> (0.41)	(0.004) <b>0.10</b> (0.17)	(0.14) <b>0.20</b> (0.26)	(0.002) <b>0.006</b> (0.012)
CONMMPOLSPC3OL_12KM_3KM	(0.79) <b>0.83</b> (0.86)	(0.97) <b>0.98</b> (0.99)	(0.82) <b>0.98</b> (1.18)	(0.08) <b>0.15</b> (0.24)	(0.19) <b>0.30</b> (0.41)	(0.04) <b>0.11</b> (0.18)	(0.19) <b>0.25</b> (0.31)	(0) <b>0.002</b> (0.003)